ADVANCED FUNCTIONAL MATERIALS
www.afm-journal.de

Nickel Silicide Nanowire Arrays for Anti-Reflective Electrodes in Photovoltaics

*Neil P. Dasgupta, Shicheng Xu, Hee Joon Jung, Andrei Iancu, Rainer Fasching, Robert Sinclair, and Fritz B. Prinz**

Conductive nanowires (NWs) provide several advantages as a template and electrode material for solar cells due to their favorable light scattering properties. While the majority of NW solar cell architectures studied are based on semiconductor materials, metallic NWs could provide equivalent anti-reflection properties, while acting as a low-resistance back contact for charge transport, and facilitate light scattering in thin layers of semiconductors coated on the surface. However, fabrication of single-crystalline highly anti-reflective NWs on low-cost, flexible substrates remains a challenge to drive down the cost of NW solar cells. In this study, metallic Ni_xSi NW arrays are fabricated by a simple, bottom-up, and low-cost method based on the thermal decomposition of silane on the surface of flexible Ni foil substrates without the need for lithography, etching or catalysts. The optical properties of these NW arrays demonstrate broadband suppression of reflection to levels below 1% from 350 nm to 1100 nm, which is among the highest values reported for NWs. A simple route to control the diameter and density of the NWs is introduced based on variations in a carrier gas flow rate. A high-resolution TEM, XRD and TEM-EDS study of the NWs reveals that they are single crystalline, with the phase and composition varying between Ni_2Si and NiSi. The nanowire resistivity is measured to be 10^{-4} Ω-cm, suggesting their use as an efficient back electrode material for nanostructured solar cells with favorable light scattering properties.

1. Introduction

Light management in photovoltaic cells is a critical area of research in order to minimize material utilization while achieving high efficiencies. By using 3-D nanostructured templates such as nanowires (NWs), the absorption length required to fully utilize the solar spectrum can be effectively decoupled from the carrier extraction length, which should be minimized to reduce recombination. Furthermore, light-scattering and trapping has been observed in 3-D architectures such as microwire,[1] nanowire,[2–5] and nanocone[6,7] arrays, allowing for enhanced absorption and suppressed reflection. This permits the use of significantly less material than a planar architecture, and reduces the purity and morphological requirements of the absorber layer due to a decreased carrier extraction length. This is the principle employed in dye-sensitized solar cells[8] (DSCs) and extremely-thin absorber[9] (ETA) cells, which utilize a very thin absorber layer in conjunction with a nanostructured template.

Ultimately, the large-scale incorporation of photovoltaics as a renewable energy source will depend on the ability to drive down costs. While nanostructured architectures can provide several benefits for solar cells, the use of top-down processing techniques involving lithography and/or etching, or catalyst-mediated growth techniques, can add significantly to the manufacturing costs. Catalyst-based techniques can also lead to incorporation of impurities into the NWs, which can negatively affect their recombination properties.[10] In this study we have grown highly-conductive (~10^{-4} Ω-cm), single-crystalline Ni_xSi NWs on flexible metal foil substrates in a completely bottom-up manner, without the need for lithography, etching or catalysts. The nanowire arrays exhibited excellent broadband anti-reflection properties, with reflection levels of less than 1% in the visible and NIR wavelengths, which is among the highest reported values for NWs. The ability to fabricate highly anti-reflective and conductive single-crystalline NWs on a low-cost and flexible substrate without any pre-patterning steps represents a powerful combination of properties to address many of the challenges associated with large-scale manufacturing of nanowire solar cells.

Many nanowire architectures have been explored for use in solar cells,[10] which are mostly based on semiconductor materials such as Si or ZnO. In this case, the nanowire serves as a component of the junction as well as a current conduction

Prof. F. B. Prinz
Department of Mechanical Engineering
Stanford University
Stanford, CA 94305, USA
E-mail: fbp@cdr.stanford.edu
Dr. N. P. Dasgupta, S. Xu, A. Iancu, Dr. R. Fasching
Department of Mechanical Engineering
Stanford University
Stanford, CA 94305, USA
H. J. Jung, Prof. R. Sinclair, Prof. F. B. Prinz
Department of Materials Science and Engineering
Stanford University
Stanford, CA 94305, USA

DOI: 10.1002/adfm.201200398

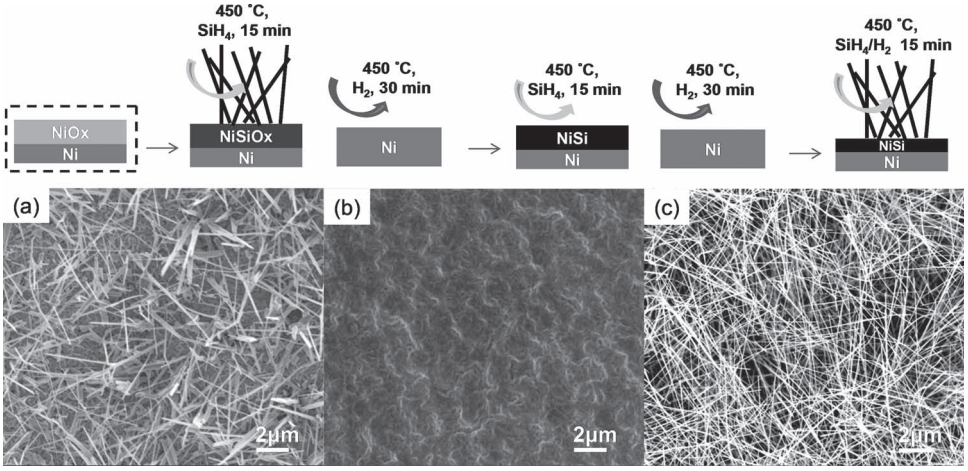

Figure 1. Schematic of nanowire growth routes and corresponding SEM images. a) Nanowire growth on an oxidized Ni surface. b) Thin film growth on a reduced Ni surface without additional carrier gas. c) Nanowire growth on a reduced Ni surface with the introduction of an additional carrier gas.

path. While doping can lead to decreased resistivity values in these semiconducting NWs, the high aspect ratio geometries and small cross-sectional areas can contribute to the series resistance of the solar cell. Furthermore, by using the nanowire as a component in the p-n junction, the choice of compatible material systems is limited. In contrast, metallic NWs can provide significantly lower resistances by acting as the back contact material, while potentially maintaining the same light-scattering benefits, and allowing for a wide variety of material combinations for the p-n junction by incorporating thin coating layers on the nanowire surface. For example, core-shell structures composed of a thin-film homojunction or heterojunction on the NW surface could be fabricated by conformally coating the surface of the metallic NW template. The NWs could also form a Schottky diode with a semiconductor material to facilitate charge separation. While carbon nanotubes[11–13] and metallic nanowires[14,15] have been studied for transparent top electrodes, there has been little reported on the use of metallic nanowire arrays for highly anti-reflective back electrodes. Among the highly-conductive nanowire materials, we have chosen to study Ni_xSi NWs due the simplicity of their fabrication methods, and favorable properties as ohmic contacts in Si-based electronics.

There are a variety of growth techniques for nickel silicide NWs, most of which can be divided into three categories:[16] delivery of silicon to nickel film,[17–22] delivery of nickel to silicon NWs,[23] and simultaneous delivery of silicon and nickel.[24,25] Some new methods, such as point contact reaction between Si and Ni NWs[26] were recently reported. Due to its simplicity and low cost, chemical vapor deposition of silane on nickel films, as the earliest discovered method,[17] has been intensively studied.

The underlying mechanism for nanowire growth based on thermal decomposition of silane on Ni films is still a matter of debate. Nickel diffusion into silicon has been proposed by several groups, and the formation of NWs rather than films has been shown to be a strong function of temperature, pressure, and silane concentration. It has been proposed that a low supersaturation degree of the vapor-phase precursors can lead to the spontaneous formation of NWs rather than thin films, due to limited nucleation kinetics.[22] The role of surface oxides on the growth has also been investigated, and it has been shown that the presence of surface oxide species can promote nanowire growth.[27,28] The surface oxide layer can serve as either a Ni diffusion barrier, or as a catalyst for a vapor-liquid-solid (VLS) growth mechanism. However, the exact role of surface oxides on nanowire growth is not clear, and several reports have been presented without the purposeful introduction of oxygen. In this study, we have successfully grown NWs on nickel surfaces with native oxide species present and after a hydrogen annealing step, suggesting that nanowire growth is possible with or without the presence of oxide species. Furthermore, a simple method to control the nanowire diameter and density is demonstrated by varying the carrier gas flow rate after first reducing the surface oxide species in the presence of hydrogen, which removes the uncertainty of NiO_x surface morphology on nanowire size.

2. Results and Discussion

The simplest route to fabricate NWs was to flow the silane gas mixture (0.84% in argon) over untreated Ni surfaces, which have a thin layer of surface oxide species present due to air exposure. Despite the simplicity of this technique, which is similar to previously reported methods, spontaneous growth of NWs was observed on the foil surface. SEM images of NWs growth by this technique are shown in **Figure 1**a. The NWs had diameters ranging from 20 to 300 nm, and lengths of 7–10 μm. It has been reported that surface oxide species can be beneficial in the growth of single crystal Ni_xSi NWs, due to limited diffusion of Ni through the NiO_x layer.[27] Additionally, the formation of $NiSi_xO_y$ species on the surface has been proposed as another contributing factor to nanowire nucleation and size.[28] The non-uniform diameters and density across the foil surface of the NWs might therefore be attributed to a variation in the size and density of the surface oxide species, which were grown by an uncontrolled oxidation process in air, and could be affected by the polycrystalline surface morphology of the Ni foils.

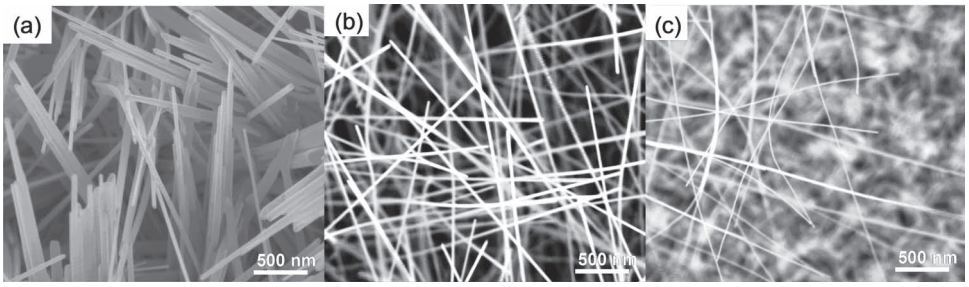

Figure 2. SEM images of NWs grown with varying hydrogen flow rates of a) 50 sccm, b) 100 sccm and c) 200 sccm.

To study the importance of surface oxides on nanowire growth, Ni foils were pre-treated by annealing the samples in hydrogen environment at 450 °C for 30 minutes to reduce the surface and eliminate the surface oxide species. As shown in Figure 1b, this resulted in the formation of a dense film rather than NWs, which further supports the hypothesis that surface oxide species are beneficial in nanowire growth.[27] However, when a stream of hydrogen or argon gas was introduced as a carrier gas at the same time as the silane, NWs formed even after an initial surface reduction, as shown in Figure 1c. This suggests that an alternate mechanism which is not dependent on the presence of oxygen species could allow for nanowire growth. While the exact mechanism for direct vapor-phase growth of NWs is oftentimes unknown, it is generally accepted that the degree of supersaturation is a critical factor in determining the growth morphology.[29] In this study, the growth of NWs versus a thin film could be affected by mass transport of the reactant species to the surface, as well as chemical kinetics of the growth process. The mass transport of silane through the surface boundary layer will be affected by an increase in the overall reactor pressure due to the introduction of the hydrogen gas stream, as well as the increased gas velocity. Also, the introduction of hydrogen can affect the equilibrium concentration of decomposed silane byproducts on the Ni surface, affecting the kinetics of the growth process. Both of these factors could affect the degree of supersaturation of the decomposed SiH_4 byproducts at the nickel surface. However, a statistical analysis of the NW diameter vs. carrier gas flow rate showed similar behavior for argon and hydrogen, suggesting that the mechanism was more dependent on total flow rate than a shift in chemical equilibrium (see supporting information).

Furthermore, the uniformity of the nanowire diameters shown in Figure 1c was significantly improved compared to the reaction with the oxidized surface. Reducing the surface before introducing silane removes the uncertainty in the oxidation state of the Ni foil, and allows for a simple and repeatable mechanism to form NWs with a uniform size distribution, as shown in Figure 1. While the use of a low-cost and flexible foil substrate has many potential advantages for large-scale photovoltaic manufacturing, the rough and polycrystalline surface could lead to concerns over the uniformity of nanowire growth based on surface oxidation. The use of a reduced surface leads to a repeatable standard which is simple to generate and results in a uniform size distribution of wires.

In addition to improved uniformity of the diameter of NWs after surface reduction, by varying the flow rate of the carrier gas, the average diameter and density of the NWs can also be controlled. **Figure 2** shows NWs grown by maintaining a constant flow rate of 100 sccm for the silane gas mixture, and varying the flow rate of the hydrogen carrier gas from 50 to 200 sccm. By simply increasing the flow rate of the carrier gas, the average diameter of the NWs could be controllably reduced.

While the details of the growth mechanism of Ni_xSi NWs are still uncertain, it can be generally separated into nucleation and growth phases. We submit the hypothesis that the progress from a thin film morphology to NWs on reduced Ni surfaces is due to variations in the nucleation behavior under different carrier gas flow rates. The nucleation of grains in the formation of a polycrystalline film on a substrate surface typically depends on the kinetics of the phase transformation. Faster solidification favors formation of a higher density of nucleation sites and smaller grains, while slower nucleation allows for growth of larger grains from initial nuclei.[30] Growth of NWs from an initial Ni_xSi seed layer on the surface suggests that nucleation and accelerated 1-D growth occurs at certain active surface sites, which could be due to defects, crystallographic domains or a variety of other factors. While the details of these nucleation and growth processes involve a complex combination of variables, we propose that by controlling the kinetics of the nucleation and solidification processes through varying the silane delivery rate to the surface, the variation in the subsequent NW diameter is likely due to smaller nucleation sites on the surface, leading to a subsequent reduction in the NW diameter. This is in agreement with the fact that the NWs are very uniform in diameter along their length, with no evidence of tapering was observed. This suggests that the diameter is determined by the size of the initial nucleation event, and rapid NW growth occurs in a 1-D fashion through Ni diffusion from the surface, as further supported by TEM-EDS data in this report.

More specifically, contributing factors to the nucleation kinetics include the rate of delivery of the decomposed silane byproducts to the surface, molar concentration of silane in the gas mixture, and overall reactor pressure. In the case of silane reaction with a nickel surface at low temperatures, the source of silicon is determined by the flux of silane to the Ni surface, where it is catalytically decomposed. Therefore, at higher flow rates, the delivery rate of Si to the surface could increase, due to a decreased laminar boundary layer thickness at increased

velocities, and improved mass transport within the furnace. The addition of an inert carrier gas also causes an increase of overall chamber pressure, for the same conductance to the vacuum pump. To maintain approximately the same partial pressure of silane in the chamber, the overall pressure was regulated by throttling a manual valve to the pump, such that the increase in overall pressure was proportional to the increase in the net flux of gas into the chamber, while maintaining the same silane flow rate. Therefore, changes in the nucleation behavior on the surface are likely due to the flow dynamics and delivery of silane to the surface, rather than an increase in the equilibrium partial pressure of silane in the gas mixture away from the surface. As the nucleation kinetics vary with the flow dynamics of the system, the diameter can be controllably varied in a systematic and simple way. As the size of the nucleation sites continues to decrease with further increasing of flow rate, the diameter continues to decrease, until eventually the growth or NWs begins to be inhibited, and the density of the wires begins to decrease along with the diameter. This suggests that an active window of carrier gas flow rate exists which promotes the formation of nucleation small nucleation sites for NWs rather than a bulk film, until the nucleation size and density decreases to the point that NW growth is no longer favorable and more sparse NW growth is observed.

The eventual decrease in NW density along with diameter with increasing flow rate has important implications for photovoltaics based on a nanowire template, as the diameter and spacing of the wires will have an effect on the optical scattering of photons,[1,3] as well as on the ability to penetrate into the nanowire array with a conformal surface coating. The proposed architectures that utilize this template would require the ability to deposit one or more thin film semiconductor coatings on the NW surface to act as the active absorber material. Therefore, depending on the deposition technique used to coat the NWs, there may be a tradeoff in effective light scattering with ability to fully penetrate into the film. One powerful technique to address this challenge is Atomic Layer Deposition (ALD), which has the ability to uniformly coat very high aspect ratio features in nanoporous substrates due to its self-limiting surface chemistry.[31] For example, this has been used to penetrate nanoporous templates based on dye-sensitized architectures.[32–34] Recently, the ability to coat NWs with single layers of PbS quantum dots by ALD by was demonstrated,[35] suggesting the ability to fabricate next-generation photovoltaic architectures on high-aspect ratio NW templates.

The ability to fabricate single-crystalline Ni_xSi NWs on Ni foil substrates provides a simple and potentially low-cost solution to creating anti-reflective bottom electrodes for photovoltaics. **Figure 3**b shows photographs of the bare Ni foil, a thin film grown on a reduced foil surface without additional carrier gas, and Ni_xSi NWs grown by a combination of silane and hydrogen on reduced surfaces. The growth of NWs led to a dramatic decrease in the surface reflectivity, and the samples appeared black, suggesting efficient reduction of surface reflectance due to light scattering from the NWs. To quantify the specular anti-reflection properties of these wires, an integrating sphere was used in conjunction with a calibrated, monochromatic light source to measure the total reflectivity. The reflectance of the three samples depicted is shown in Figure 3a. The bare Ni foil

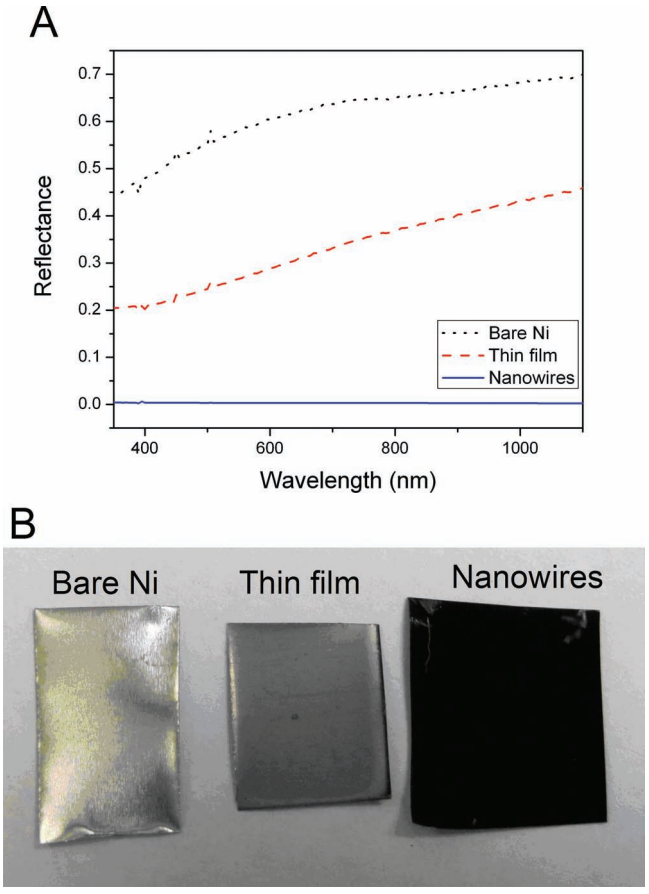

Figure 3. a) Reflectance data measured by an integrating sphere, showing a decrease in reflectance from the bare Ni foil, to the thin film, to the nanowire arrays. b) Photograph of the three samples shown in the reflectivity data, showing a dramatic decrease in reflectivity of the nanowire sample.

was highly reflective, with a reflectance varying from 45–70% in the wavelength range of 350–1100nm. The thin film exhibited a lower reflectance than the metal surface, but still exhibited significant reflectivity in the visible wavelengths. The nanowire sample exhibited excellent anti-reflection properties, with less than 1% reflection measured across the range of wavelengths considered. As the transmission through the thick Ni foil was negligible, this represents greater than 99% absorption in this nanowire array, which is among the highest reported values for nanostructured templates. This is particularly remarkable, given the random orientation of the nanowires, as ordering of the nanowires has been shown to be beneficial for light trapping.[1,5,10] While this random orientation may make penetration of the films difficult for line-of-sight deposition techniques, processes such as ALD should have no problem uniformly coating these structures to create core-shell wires. The excellent anti-reflection properties of these metallic nanowire arrays could allow for such ultra-thin coatings to be applied using a variety of material systems to facilitate carrier generation and separation, while minimizing material utilization and the diffusion length associated with charge separation. This will require careful selection of the dielectric properties of the coating

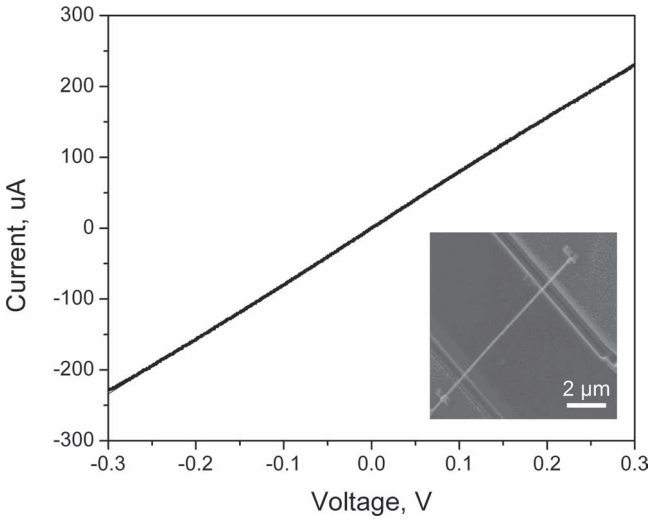

Figure 4. Current vs. voltage profile of a single nanowire contacted by two Ni electrodes, as shown in the SEM image in the insert.

material, such that the majority of light is absorbed in the semiconductor before excessive parasitic absorption occurs in the metallic NWs, while maintaining the desirable light scattering properties of the underlying template structure.

In addition to excellent reflection suppression, the use of Ni_xSi nanowire arrays has a significant advantage as a bottom electrode material due to the metallic nature of the wires. For example, by using a metallic NW as the core material in a core-shell structure, series resistance and transport losses along the wire could be reduced compared to a purely semiconducting NW system. Pure NiSi NWs grown by deposition of Ni metal onto single-crystal Si NWs were reported to have a resistivity of about 10^{-5} Ω–cm.[23] While the NWs grown in this report were also single-crystalline, we expect that variations in stoichiometry and phase, may lead to a reduction in conductivity. To quantify the resistivity of these NWs, the I–V spectrum of a single wire grown by the reduced-surface route was measured using a 2-point method using nickel electrodes.

Figure 4 shows a linear I–V behavior of the nanowire, with a resistance of 1285 Ω. The nanowire diameter was measured to be 80 nm with a 6 μm gap between the electrodes. The lead resistance of the electrodes was measured to be 2.62 Ω, so neglecting this effect the nanowire resistivity was calculated to be 1.07×10^{-4} Ω-cm. This is likely to be an upper limit to the actual nanowire resistivity, as contact resistances may have contributed further to the signal, especially since any surface oxidation of the nanowire was not removed prior to measurement.[24] The linear I–V behavior also indicates that an ohmic contact is formed between nickel metal and the NWs, which indicates that the electrical contact to the foil substrate should be favorable. The combination of this high conductivity and low reflectivity based on such a simple bottom-up fabrication scheme presents a powerful combination of characteristics for large-scale photovoltaic electrode manufacturing.

In order to study the crystallographic and chemical properties of the NWs, high-resolution transmission electron microscopy (HRTEM) analysis was performed. HRTEM images of two different NWs show single-crystalline orthorhombic Ni_3Si_2 in the [110] zone orientation in **Figure 5**a and single-crystalline hexagonal Ni_2Si in the $[2\bar{1}\bar{1}0]$ zone orientation in Figure 5b. The measured interplanar d-spacings of Ni_3Si_2 (d_{001} = 6.92 Å, d_{110} = 8.10 Å) and Ni_2Si ($d_{01\bar{1}0}$ = 3.32 Å, d_{0001} = 4.89 Å) are consistent with the calculated d-spacings of Ni_3Si_2 (d_{001} = 6.920 Å, d_{110} = 8.117 Å) and Ni_2Si ($d_{01\bar{1}0}$] = 3.295 Å, d_{0001} = 4.890 Å) from previously reported values[36–38] [Ni_3Si_2 (a = 12.290 Å, b = 10.810 Å, c = 6.98 Å, orthorhombic, $Cmc2_1$), Ni_2Si (a = 4.890 Å, c = 3.295 Å, hexagonal, $C6_3/m$)]. For visualization purposes, the theoretical projection of these two crystal structures are shown in Figure 5c and 5d, respectively.

The resemblance of the projected structure and the image for Ni_2Si is quite good, but clearly the Ni_3Si_2 structure is more complex. Many factors contribute to discrepancies between the theoretical and measured crystal structures. One important influence is that the measured lattice parameter changes slightly along the length of the wire. This can induce some strain and distortion of the lattice, which can lead to differences in theoretical projections of the atomic positions and the actual HRTEM images. Additionally, differences in measured and theoretical values can stem from unresolved Ni and Si atoms due to the resolution limit of the TEM (1.4 ~ 1.5 Å at 200kV e-beam acceleration), as well as from phase contrast change by defocus (focal plane position on the TEM sample) and local thickness variation.

To further study the phases present in the NWs, x-ray diffraction (XRD) and TEM-EDS (energy dispersive spectroscopy) were performed. To prepare the samples for XRD analysis, the foil-nanowire samples were immersed in toluene and placed in an ultrasonic bath to detach the NWs from the foil surface. This nanowire solution was subsequently drop cast onto glass slides, and the toluene was evaporated leaving an ensemble of NWs on the glass surface. By performing XRD on these samples, the phases present in a large ensemble of wires could be studied without any background signal from the foil substrate. The results of the XRD scans for NWs grown the oxidized and reduced Ni foil surfaces are shown in **Figure 6**a. Several phases were observed in the XRD spectra, with the most notable phase being orthorhombic Ni_3Si_2. Additionally, orthorhombic NiSi and hexagonal Ni_2Si peaks were observed. The XRD spectrum for NWs grown the oxidized and reduced surface were similar, suggesting that the nanowire phase was not strongly dependent on the surface pre-treatment.

To study the chemical composition of the wires, local EDS spectra (diameter~500nm) were measured at various points of two different NWs, as indicated by the circled regions in Figure 6b and 6c. As shown in the TEM-EDS analysis (see supporting information), the chemical composition of the NWs changes 2 ~ 5% along the length of the wire with Ni content decreasing in the growth direction, presumably due to Ni diffusion from the foil into the nanowire. This trend was observed in NWs growth with both oxidized [Figure 6b] and reduced [Figure 6c] surfaces, which further suggests that the growth of the NW is due to nickel diffusion from the substrate into the wire in both cases, and differences in the diameter and density of the wires was due to variations in the initial nucleation sites of the NWs on the surface rather than a fundamentally different growth mechanism. This

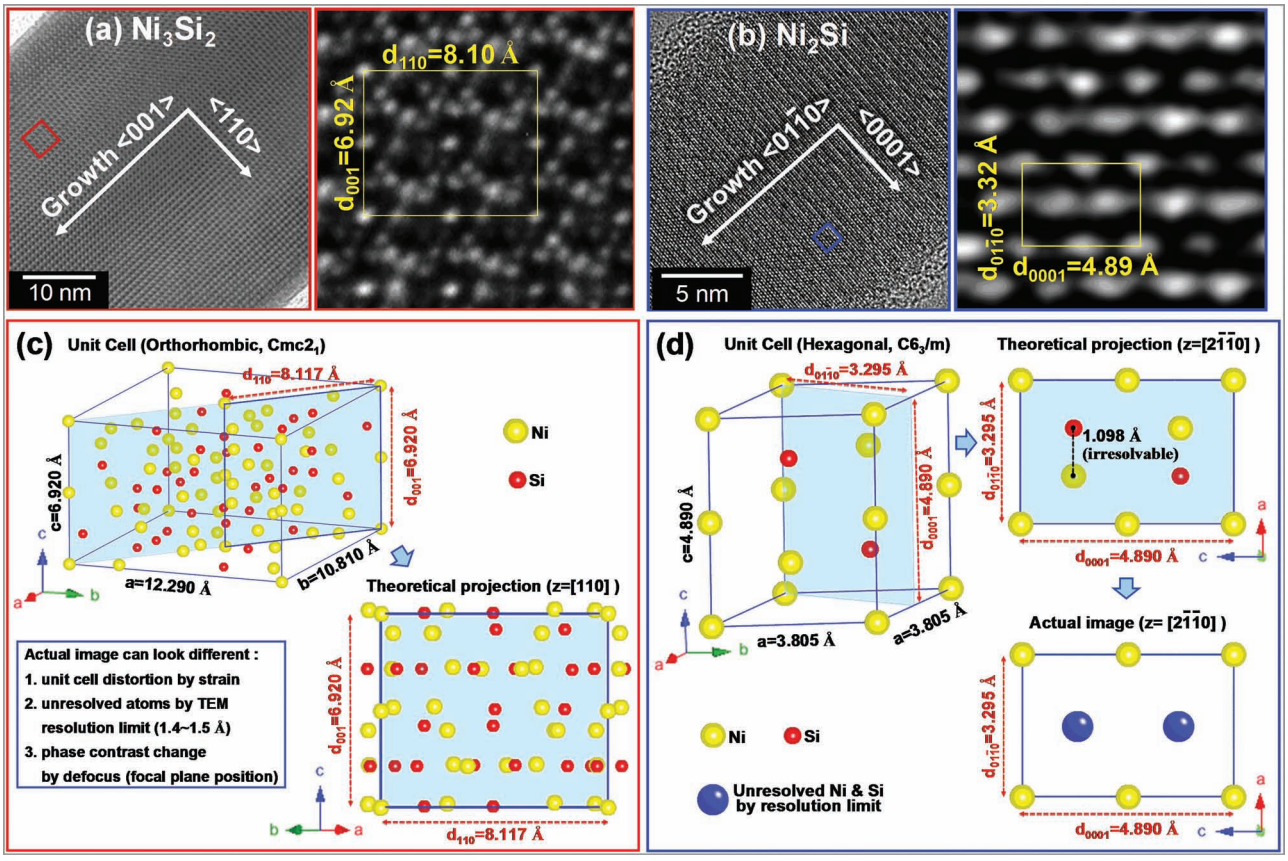

Figure 5. HRTEM images and theoretical projection analyses of two different NWs. The phase observed was Ni_3Si_2 (a & c) and Ni_2Si (b & d). Each right side TEM image is digitally enlarged from the boxed region on each left side image. The theoretical projection of Ni and Si atoms in different zone axis orientations (z = [110] for Ni_3Si_2 (b) and z = [2 $\bar{1}\bar{1}$ 0] for Ni_2Si (d)) are generated from multiple arrays of 3D unit cells.

could lead to a phase variation (i.e. structure change by lattice strain) within a single NW along the length of the wire, although the wires appeared to be single-crystalline in the HRTEM images. Energy-filtered TEM (EFTEM) images for Ni and Si atoms confirm that the majority of the regions in the NW show a very uniform concentration profile (see supporting information). However, a few selective regions show an abrupt change of Ni and Si concentration, which may be the point of a phase variation. This variation in phase and composition along the wire could have implications for the conductivity of the wires, as the electron mobility will also likely vary along the length of the wire.

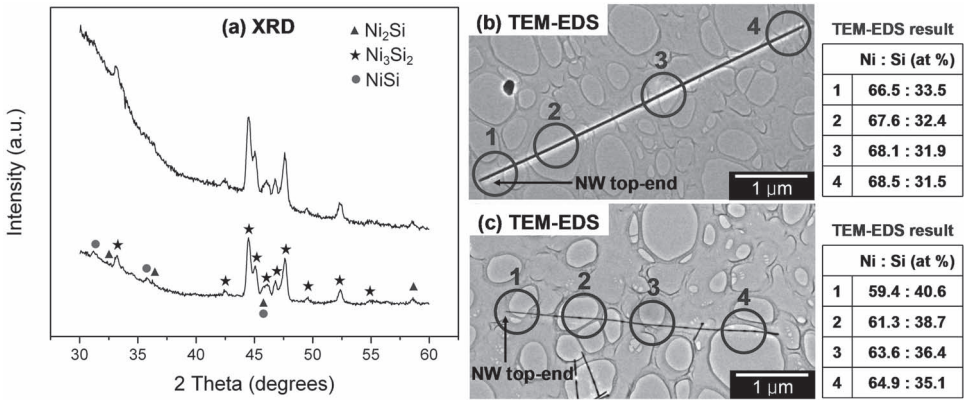

TEM-EDS result	Ni : Si (at %)
1	66.5 : 33.5
2	67.6 : 32.4
3	68.1 : 31.9
4	68.5 : 31.5

TEM-EDS result	Ni : Si (at %)
1	59.4 : 40.6
2	61.3 : 38.7
3	63.6 : 36.4
4	64.9 : 35.1

Figure 6. XRD spectra of NWs growth on b) oxidized (top) and reduced (bottom) Ni surfaces in, and TEM-EDS results from local regions (circles) on different NWs grown on b) oxidized and c) reduced Ni surfaces.

3. Conclusions

The ability to fabricate metalic, single crystalline NWs on low-cost and flexible metal foil substrates is a powerful technique for electrode fabrication. In this study, we have introduced a simple method to repeatably prepare the surface of Ni foils for Ni_xSi nanowire growth by reduction in a hydrogen environment, followed by introduction of silane with an additional carrier gas. The diameter and density of the wires can be easily controlled by varying the carrier gas flow rate. The nanowire arrays demonstrate excellent anti-reflection properties, and high electrical conductivity (10^{-4} Ω-cm) suggesting their use as a light-scattering back electrode for photovoltaics which could be coated with a variety of semiconductor material systems with reduced purity and absorptivity requirements. The combination of high conductivity, excellent light-scattering properties and a simple, bottom-up fabrication make this an attractive template for a variety of 3-D photovoltaic architectures.

4. Experimental Section

Ni_xSi NWs were grown on Ni foil substrates (Aldrich, 99.9%) in a tube furnace. The tube was purged with high purity argon, and pumped down to a base pressure of 10^{-3} Torr prior to the deposition. The oxidized Ni surface was either left untreated, or reduced in hydrogen at 450 °C for 30 min to remove the surface oxide species. NWs were grown by flowing a low-concentration silane gas mixture (0.84% in argon) at a temperature of 450 °C for 30 min. The use of this low-concentration gas mixture is below the flammability limit of silane, which could further reduce cost and safety issues in manufacturing settings. Additionally, hydrogen or argon was used as a carrier gas in some experiments involving reduced surfaces, to study the effect of carrier gas flow rate on NW size and density.

SEM images were taken with a FEI Strata 235 Dual-Beam focused ion beam (FIB) system. Reflectivity measurements were performed with a Newport silicon photodetector (918D series) in conjunction with an Oriel barium sulfate coated integrating sphere and a calibrated, monochromated light source. The sample was placed in the middle of the integrating sphere, and an angle of incidence of ~10° was maintained relative to normal to minimize specular reflection through the small entrance to the sphere where the light source entered.

For the electrical resistivity measurement, Ni electrodes were patterned by traditional photolithography, and a single nanowire was transferred to the electrodes using an omniprobe transfer method in the same Focused ion beam (FIB) system and attached using ion-beam induced deposition of Pt (see supporting information). A Keithley 2636A Source Measure Unit (SMU) was used in conjunction with Cascade Microtech DC microprobes to determine the I–V characteristics of the single nanowire.

HRTEM analysis was performed using a FEI 80–300 Titan operated at an accelerating voltage of 300 kV for Figure 5a and a FEI Tecnai G2 F20 X-TWIN operated at an accelerating voltage of 200 kV for Figure 5b. TEM-EDS and EFTEM analysis was performed in the same Tecnai system at an accelerating voltage of 200 kV. Every EDS spectrum was acquired for a duration of 60 s. The beam width was focused to ~500 nm.

To prepare the samples for XRD analysis, the foil-nanowire samples were immersed in toluene and placed in an ultrasonic bath to detach the NWs from the foil surface. This nanowire solution was subsequently drop cast onto glass slides, and the toluene was evaporated leaving an ensemble of NWs on the glass surface. By performing XRD on these samples, the phases present in a large ensemble of wires could be studied without any background signal from the foil substrate. XRD measurements were performed with a PANalytical X'Pert PRO x-ray diffraction system by scanning 2θ from 30–60° at a fixed omega angle of 1.5°.

Supporting Information

Supporting Information is available from the Wiley Online Library or from the author.

Acknowledgements

H. J. J. was supported as part of the Center on Nanostructuring for Efficient Energy Conversion (CNEEC) at Stanford University, an Energy Frontier Research Center funded by the U.S. Department of Energy, Office of Science, Office of Basic Energy Sciences under Award # DE-SC0001060. N. P. D. acknowledges support from the U.S. Department of Energy, Office of Energy Efficiency and Renewable Energy (EERE) Postdoctoral Research Awards under the SunShot Solar Energy Technologies Program. The authors acknowledge use of the facilities at the National Center for Electron Microscopy, Lawrence Berkeley Lab, supported by the U.S. Department of Energy under Contract # DE-AC02-05CH11231. Supporting Information is available online from Wiley InterScience or from the author.

Received: February 9, 2012
Revised: March 9, 2012
Published online: May 18, 2012

[1] M. D. Kelzenburg, S. W. Boettcher, J. A. Petykiewicz, D. B. Turner-Evans, M. C. Putnam, E. L. Warren, J. M. Spurgeon, R. M. Briggs, N. S. Lewis, H. A. Atwater, *Nat. Mater.* **2010**, *9*, 239.
[2] L. Tsakalakos, J. Balch, J. Fronheiser, B. A. Borevaar, O. Sulima, J. Rand, *Appl. Phys. Lett.* **2007**, *91*, 233117.
[3] L. Hu, G. Chen, *Nano Lett.* **2007**, *7*, 3249.
[4] O. L. Muskens, J. G. Rivas, E. A. Rienk, E. P. A. M. Bakkers, A. Lagendijk, *Nano Lett.* **2008**, *8*, 2638.
[5] E. Garnett, P. Yang, *Nano Lett.* **2010**, *10*, 1082.
[6] J. Zhu, J. Yu, G. F. Burkhard, C.-M. Hsu, S. T. Connor, Y. Xu, Q. Wang, M. McGehee, S. Fan, Y. Cui, *Nano Lett.* **2009**, *9*, 279.
[7] J. Zhu, C.-M. Hsu, Z. Yu, S. Fan, Y. Cui, *Nano Lett.* **2010**, *10*, 1979.
[8] B. O'Regan, M. Grätzel, *Nature* **1991**, *353*, 737.
[9] I. Kaiser, K. Ernst, C. H. Fischer, R. Konenkamp, C. Rost, I. Sieber, M. C. Lux-Steiner, *Sol. Energy Mater. Sol. Cells* **2001**, *67*, 89.
[10] E. C. Garnett, M. L. Brongersma, Y. Cui, M. C. McGehee, *Annu. Rev. Mater. Res.* **2011**, *41*, 269.
[11] A. D. Pasquier, H. E. Unalan, K. Alokik, S. Miller, M. Chhowalla, *Appl. Phys. Lett.* **2005**, *87*, 203411.
[12] M. W. Rowell, M. A. Topinka, M. D. McGehee, H.-J. Prall, G. Dennler, N. S. Sariciftci, L. Hu, G. Gruner, *Appl. Phys. Lett.* **2006**, *88*, 233506.
[13] J. van de Lagemaat, T. M. Barnes, G. Rumbles, S. E. Shaheen, T. J. Coutts, C. Weeks, I. Levitsky, J. Peltola, P. Glatkowski, *Appl. Phys. Lett.* **2006**, *88*, 233503.
[14] J.-Y. Lee, S. T. Connor, Y. Cui, P. Peumans, *Nano Lett.* **2008**, *8*, 689.
[15] S. De, T. M. Higgins, P. E. Lyons, E. M. Doherty, P. N. Nirmalraj, W. J. Blau, J. J. Boland, J. N. Colman, *ACS Nano* **2009**, *3*, 1767.
[16] A. L. Schmitt, J. M. Higgins, J. R. Szczech, S. Jin, *J. Mater. Chem.* **2010**, *20*, 223.
[17] C. A. Decker, R. Solanki, J. L. Freeouf, J. R. Carruthers, D. R. Evans, *Appl. Phys. Lett.* **2004**, *84*, 1389.
[18] X. Q. Yan, H. J. Yuan, J. X. Wang, D. F. Liu, Z. P. Zhou, Y. Gao, L. Song, L. F. Liu, W. Y. Zhou, G. Wang, S. S. Xie, *Appl. Phys. A.* **2004**, *79*, 1853.
[19] J. Kim, W. A. Anderson, *Thin Solid Films* **2005**, *483*, 60.
[20] J. Kim, W. A. Anderson, Y.-J. Song, G. B. Kim, *Appl. Phys. Lett.* **2005**, *86*, 253101.
[21] C.-J. Kim, K. Kang, Y. S. Woo, K.-G. Ryu, H. Moon, J.-M. Kim, D.-S. Zang, M.-H. Jo, *Adv. Mater.* **2007**, *19*, 3637.

[22] K. Kang, C.-J. Kim, M.-H. Jo, *J. Appl. Phys.* **2009**, *105*, 122407.
[23] Y. Wu, J. Xiang, C. Yang, W. Lu, C. M. Lieber, *Nature* **2004**, *430*, 61.
[24] Y. Song, A. L. Schmitt, S. Jin, *Nano Lett.* **2007**, *7*, 965.
[25] C.-Y. Lee, M.-P. Lu, K.-F. Liao, W.-F. Lee, C.-T. Huang, S.-Y. Chen, L.-J. Chen, *J. Phys Chem. C* **2009**, *113*, 2286.
[26] K.-C. Lu, W.-W. Wu, H.-W. Wu, C. M. Tanner, J. P. Chang, L. J. Chen, K. N. Tu, *Nano Lett.* **2007**, *7*, 2389.
[27] K. Kang, S.-K. Kim, C.-J. Kim, M.-H. Jo, *Nano Lett.* **2008**, *8*, 431.
[28] Z.-Q. Sun, S.-J. Whang, W.-F. Yang, S.-J. Lee, *Jpn. J. Appl. Phys.* **2009**, *48*, 04C138.
[29] Y. Xia, P. Yang, Y. Sun, Y. Wu, B. Mayers, B. Gates, Y. Yin, F. Kim, H. Yan, *Adv. Mater.* **2003**, *15*, 353.
[30] C. Spinella, S. Lombardo, F. Priolo, *J. Appl. Phys.* **1998**, *84*, 5383.
[31] S. M. George, *Chem. Rev.* **2010**, *110*, 111.
[32] M. Law, L. E. Greene, A. Radenovic, T. Kuykendall, J. Liphardt, P. Yang, *J. Phys. Chem. B* **2006**, *110*, 22652.
[33] A. B. F. Martinson, J. W. Elam, J. T. Hupp, M. J. Pellin, *Nano Lett.* **2007**, *7*, 2183.
[34] T. W. Hamann, A. B. F. Martinson, J. W. Elam, M. J. Pellin, J. T. Hupp, *Adv. Mater.* **2008**, *20*, 1560.
[35] N. P. Dasgupta, H. J. Jung, O. Trejo, M. T. McDowell, A. Hryciw, M. Brongersma, R. Sinclair, F. B. Prinz, *Nano Lett.* **2011**, *11*, 934.
[36] G. Pilström, *Acta Chem. Scand.* **1961**, *15*, 893.
[37] D. Borivent, B. Billia, J. Paret, *J. Appl. Phys.* **2008**, *104*, 013523.
[38] F. Bosselet, J. C. Viala, C. Colin, B. F. Mentzen, J. Bouix, *Mater. Sci. Eng. A* **1993**, *167*, 147.